Available online at www.sciencedirect.com

ScienceDirect

Publishing Services by Elsevier

International Journal of Naval Architecture and Ocean Engineering 9 (2017) 35–44
http://www.journals.elsevier.com/international-journal-of-naval-architecture-and-ocean-engineering/

Drag reduction of a rapid vehicle in supercavitating flow

D. Yang [a], Y.L. Xiong [b,c,*], X.F. Guo [d]

[a] School of Naval Architecture and Ocean Engineering, Huazhong University of Science & Technology, Wuhan, 430074, China
[b] School of Civil Engineering and Mechanics, Huazhong University of Science & Technology, Wuhan, 430074, China
[c] Hubei Key Laboratory of Engineering Structural Analysis and Safety Assessment, Luoyu Road 1037, Wuhan, 430074, China
[d] The Second Institute of Huaihai Industrial Group, Changzhi, 046000, China

Received 13 November 2015; revised 13 May 2016; accepted 12 July 2016
Available online 9 August 2016

Abstract

Supercavitation is one of the most attractive technologies to achieve high speed for underwater vehicles. However, the multiphase flow with high-speed around the supercavitating vehicle (SCV) is difficult to simulate accurately. In this paper, we use modified the turbulent viscosity formula in the Standard K-Epsilon (SKE) turbulent model to simulate the supercavitating flow. The numerical results of flow over several typical cavitators are in agreement with the experimental data and theoretical prediction. In the last part, a flying SCV was studied by unsteady numerical simulation. The selected computation setup corresponds to an outdoor supercavitating experiment. Only very limited experimental data was recorded due to the difficulties under the circumstance of high-speed underwater condition. However, the numerical simulation recovers the whole scenario, the results are qualitatively reasonable by comparing to the experimental observations. The drag reduction capacity of supercavitation is evaluated by comparing with a moving vehicle launching at the same speed but without supercavitation. The results show that the supercavitation reduces the drag of the vehicle dramatically.

Keywords: Drag reduction; Numerical simulation; Supercavitation; Underwater vehicle; Turbulent model; Multiphase flow; High-speed torpedo; Supercavitating vehicle; Computational fluid dynamics; Cavitation number

1. Introduction

Hydrodynamic drag is one of the greatest interests in marine hydrodynamics and aerodynamics. For a moving vehicle, drag force on one hand induces a lot of energy consumption in our daily life. On the other hand, it limits the speed of the vehicle. In addition, the drag force of a stationary object enhances structural load, which is often accompanied with high cost during the design process to maintain the structure strength. As a consequence, drag reduction is a long-standing challenge for both scientists and engineers. A series of flow control methods have been put forward for decreasing drag, such as putting tiny amount of polymer additives into water (Xiong et al., 2010; Xiong et al., 2013), using porous media (Bruneau and Mortazavi, 2008), as well as shape optimization (Bruneau et al., 2013), and so on (Beaudoin and Aider, 2008; Choi et al., 2008). One of the most promising ways to reduce drag resistance is by filling water vapour or gas to isolate the underwater vehicle, one of which is well known as supercavitating drag reduction (Arndt et al., 2005; Ceccio, 2010; Arndt, 2013). In a supercavitating flow, the cavitator contacts with water constantly. The rest parts of the vehicle mostly contact with either the saturated water vapour produced by natural phase exchange or the gas releases from an artificial ventilation vent. Since the surface of underwater vehicle contact with vapour or gas, the friction drag exerted on the vehicle is negligible. Therefore, the vehicle could achieve very high speed in water. This technology supplies us an alternative of high speed voyage in the future.

* Corresponding author. School of Civil Engineering and Mechanics, Huazhong University of Science & Technology, Wuhan, 430074, China.
E-mail address: xylcfd@hust.edu.cn (Y.L. Xiong).
Peer review under responsibility of Society of Naval Architects of Korea.

http://dx.doi.org/10.1016/j.ijnaoe.2016.07.003

However, it should be noted that this technique is still in the very early stage even though it has been utilized in the so-called supercavitating torpedo (Choi et al., 2005a,b; Alyanak et al., 2006). There are several challenges need to be overcome in order to achieve manipulated flight in the water: 1) the balance of the gravity of the vehicle is difficult since the Archimedes force is becoming negligible because the vehicle is enveloped by low-density medium; 2) the traditional propeller is ineffective since it is difficult to extend the turbine into water in order to get thrust by pushing water; 3) it is hard to control the moving direction of the underwater vehicle; 4) how to isolate the tremendous noise aroused by the condensation of bubbles; 5) how to brake the vehicle safely. All of the above questions are related to the fundamental problems, which are among how to calculate the unsteady pressure drag on the cavitator, as well as the shape and size of the cavity accurately, and how to optimize the shape of cavitator to achieve less drag but larger cavity.

To solve these problems, both the potential theory and Computational Fluid Dynamics (CFD) are utilized to calculate the shape of the cavity and the corresponding drag (Dieval et al., 2000; Choi et al., 2005b; Alyanak et al., 2006; Gao et al., 2012; Likhachev and Li, 2014; Pan and Zhou, 2014). Furthermore, there are also a great number of the semi-empirical theories and experimental studies have been done on the supercavitating flow (Tulin, 1998; Hrubes, 2001; Ito et al., 2002; Kulagin, 2002; Nouri and Eslamdoost, 2009; Yi et al., 2009; Cameron et al., 2011; Kim and Kim, 2015). In general, the semi-empirical theory and the potential theory could give an accurate result quickly, however they are not so versatile for the transient flow and complex geometric configuration. Meanwhile they are incapable to give detailed flow behaviour of the cavitation (Tulin, 1998; Kim and Kim, 2015). On the contrary, CFD and the experimental measurements are flexible to obtain abundant results, but they are both time-consuming and hard to implement. Especially, the cavitation model, multiphase flow method, numerical methods, and the turbulence model influence the accuracy of the result (Singhal et al., 2002; Coutier-Delgosha et al., 2007; Seif et al., 2009).

In this manuscript, we are going to examine our numerical results by experimental data, and then we are going to study the drag coefficient of different cavitators by numerical simulations. In the last part of the paper, the supercavitating drag reduction capacity is compared by using an unsteady numerical simulation. The selected case corresponds to our outdoor supercavitating experiment.

2. Governing equations and computational setup

A single fluid approach was used to simulate the unsteady flow of mixture phase consisting of vapour phase and water phase. The governing equations which are composed by mass and momentum conservation equations as well as a transport equation of water vapour have the following form, respectively:

$$\frac{\partial}{\partial t}(\rho_m) + \nabla \cdot \left(\rho_m \vec{v}_m\right) = \dot{m} \tag{1}$$

$$\frac{\partial}{\partial t}\left(\rho_m \vec{v}_m\right) + \nabla \cdot \left(\rho_m \vec{v}_m \vec{v}_m\right) = -\nabla p + \nabla \cdot \left[\mu_m\left(\nabla v_m + \nabla v_m^T\right)\right] \tag{2}$$

$$\frac{\partial}{\partial t}(\rho_m f) + \left(\rho_m \vec{v}_v f\right) = \nabla(\gamma \nabla f) + R_e - R_c \tag{3}$$

Here $\vec{v}_m = \sum_{k=1}^{2} \alpha_k \rho_k \vec{v}_k / \rho_m$ is the averaged velocity of mass; α_k denotes a volume fraction of phase-k, the subscript k and m represent the phase-k and mixture phase, respectively. The mixture density and viscosity are calculated by $\rho_m = \sum_{k=1}^{2} \alpha_k \rho_k$ and $\mu_m = \sum_{k=1}^{2} \alpha_k \mu_k$. The mass fraction of water vapour f can be calculated based on the density relation as $1/\rho_m = f/\rho_v + (1-f)/\rho_l$, the suffix of m, l and v denote the mixture, liquid and vapour phase, respectively. To improve the numerical stability, an artificial diffusion term in the transport equation is employed; the diffusion coefficient is reasonable small and may avoid a sharp interface which arises remarkable numerical instability in cavitating simulation. The source term R_e and R_c in the transport equation represent the generation and condensation of vapour, respectively. Source terms are sensitive to the local absolute static pressure and turbulent kinetic energy. Here we adopted the Singhal's cavitation model which has the following form:

$$\text{if } p \le p_v: \quad R_e = C_e \frac{V_{ch}}{\zeta} \rho_l \rho_v \sqrt{\frac{2(p_v - p)}{3\rho_l}} (1-f) \tag{4}$$

$$\text{else if } p > p_v: \quad R_c = C_c \frac{V_{ch}}{\zeta} \rho_l \rho_v \sqrt{\frac{2(p - p_v)}{3\rho_l}} f \tag{5}$$

where p_v is the phase change threshold pressure which is calculated by $p_v = p_{sat} + 0.5 p_{turb}$ and $p_{turb} = 0.39\rho_m k$, here k is the turbulent kinetic energy. V_{ch} is a characteristic velocity which measure the effect of local relative velocity between liquid and vapour and is estimated as $\sqrt{k}$. The empirical coefficient C_e and C_c are set as 0.02 and 0.01, respectively, as recommended in the literature (Singhal et al., 2002). ζ is the surface tension of liquid.

For the most circumstances, cavitating flows are also turbulent flow, which are characterized by fluctuating velocity fields. Since these fluctuations can be of small scale and high frequency, they are too computationally expensive to simulate directly in practical engineering applications. Instead, the instantaneous (exact) governing equations can be time-averaged, ensemble-averaged, or otherwise manipulated to remove the small scales, resulting in a modified set of equations which are computationally less expensive to solve. To model the influence of turbulence in the present study, the *SKE* two equations model as well as standard wall function are utilized in our simulations. The two equations are written as follows:

$$\rho_m\frac{\partial k}{\partial t}+\rho_m v_j\frac{\partial k}{\partial x_j}=\frac{\partial}{\partial x_j}\left[\left(\mu_m+\frac{\mu_t}{\sigma_k}\right)\frac{\partial k}{\partial x_j}\right]+\mu_t\frac{\partial v_j}{\partial x_i}\left(\frac{\partial v_j}{\partial x_i}+\frac{\partial v_i}{\partial x_j}\right)-\rho_m\varepsilon \tag{6}$$

$$\rho_m\frac{\partial \varepsilon}{\partial t}+\rho_m v_k\frac{\partial \varepsilon}{\partial x_k}=\frac{\partial}{\partial x_k}\left[\left(\mu_m+\frac{\mu_t}{\sigma_\varepsilon}\right)\frac{\partial \varepsilon}{\partial x_k}\right]+\frac{c_1\varepsilon}{k}\mu_t\frac{\partial v_i}{\partial x_j}\left(\frac{\partial v_i}{\partial x_j}+\frac{\partial v_j}{\partial x_i}\right)-c_2\rho_m\frac{\varepsilon^2}{k} \tag{7}$$

and $c_\mu=0.09, c_1=1.44, c_2=1.92, \sigma_k=1.0, \sigma_\varepsilon=1.3$.

It is still a numerical challenge to achieve an accurate converged solution for high-speed supercavitating flow, because of the huge density ratio of liquid to vapour, the severe pressure gradient and complex mass and momentum exchanges between different phases. In addition, it is normal to generate a poor quality mesh with high skewness considering the complexity of geometry for the purpose of engineering design. Then it would be very difficult to obtain proper numerical results by the reason of 'blowing-up'. During our numerical simulations, we employed the SKE, which is the most widely-used engineering turbulence model for industrial applications. It is well known for its robustness. However, the turbulent viscosity ratio by using SKE is extremely high, it also affects the convergence of the solution. Furthermore, the model itself is unable to simulate the unsteady behaviour of cavitation correctly. After an initial fluctuation of the cavity volume, the calculation leads to a quasi-steady behaviour of the cavitation sheet. Moreover, the overall length of the predicted cavity is shorter than the experimental result. The problem seems to lie in the over prediction of the turbulent viscosity in the region of the cavity closure. The re-entrant jet formation, which is the main cause for the cavitation cloud separation, does not take place in this case.

Therefore, it is reasonable to adjust the SKE model. However, the turbulence modelling of multiphase flows is challenging. Considering the limitation of the SKE model, it overestimate the production of k unphysically in the region where strain rate is large. This is a very severe error which may change the pressure threshold of cavitation (recall that isotropic normal Reynolds stress is $2\rho k/3$). Furthermore, as one of the eddy viscosity models, isotropic assumption is built in SKE model, which is not the fact of supercavitating flow, especially for those regions with both phases (where have anisotropic material properties). Hence turbulent model were frequently corrected to fit special flows in literature. Here we modified the turbulent viscosity formula to avoid an overestimation of k and turbulent viscosity ratio for the region with both liquid and vapour phase. The current correction of SKE could suppress turbulent viscosity ratio and facilitate the convergence of a solution for supercavitating flow. Specifically, to avoid the overestimation of the turbulent viscosity ratio, a function of $f(\rho)=\left[\exp\left(\frac{4(\rho_m-\rho_v)(\rho_m-\rho_l)}{\rho_l^2}\right)\right]\rho_m$ is utilized instead of using the standard form $f(\rho)=\rho_m$ in SKE two equations model. Therefore, the turbulent viscosity in this study is given by:

$$\mu_t=\left[\exp\left(\frac{4(\rho_m-\rho_v)(\rho_m-\rho_l)}{\rho_l^2}\right)\right]\rho_m C_\mu\frac{k^2}{\varepsilon} \tag{8}$$

Either in liquid or vapour, the corrected model recovers to the original SKE model. For the mixture zone of vapour and liquid, the turbulent viscosity is reduced in the corrected model. The reduction of turbulent viscosity can be illustrated as shown in Fig. 1.

The above non-linear system is discretized to the algebraic equations with a finite volume method. The linear algebraic system is solved under a W-type multi-grid to accelerate convergence. According to the reference (Seif et al., 2009), PISO method was used in this study for the coupling between pressure and velocity.

3. Numerical validation

The basic similarity parameters of the supercavitation flows are cavitation number and Reynolds number, which are defined as:

$$\sigma=\frac{P_\infty-P_c}{\frac{1}{2}\rho_l V_\infty^2},\ \text{and}\ \mathrm{Re}=\frac{\rho_l V_\infty D}{\mu_l} \tag{9}$$

where p_∞ is the environmental pressure; p_c is the pressure inside of a cavity;ρ_l andμ_l denote the density and viscosity of liquid phase, respectively; and V_∞ is the relative velocity of bulk liquid to the SCV. Cavitation number expresses the relationship between the difference of the local absolute pressure to the saturated vapour pressure at present temperature and the kinetic energy per volume, and it is used to characterize the potential of the flow to cavitate. To validate the present numerical method and model, cavitating flows past a slender body with a half-sphere cavitator and a 45-degree

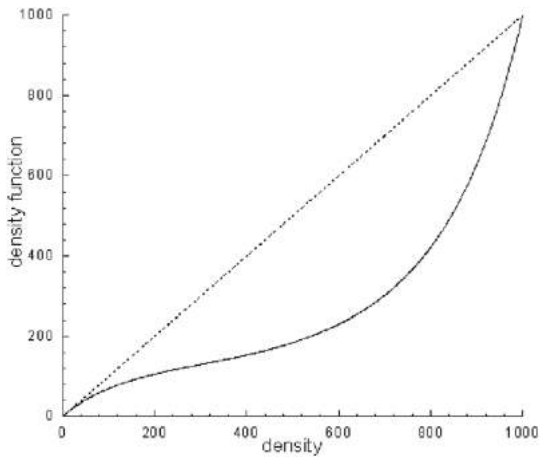

Fig. 1. The modification of the density function in SKE two equations model. The solid line represents the corrected model, the dotted line is the standard form.

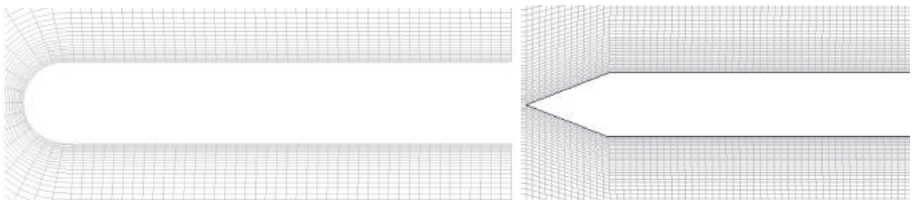

Fig. 2. Partial mesh around slender body with half-sphere cavitator (left) and 45-degree cone cavitator.

cone cavitator are studied. The partial mesh configurations around the slender bodies are shown in Fig. 2.

Figs. 3 and 4 plot the pressure coefficient $\left(c_p = \frac{2(p-p_\infty)}{\rho_l V_\infty^2}\right)$ along the surface of the slender body for the cases with a half-sphere cavitator and a 45-degree cone cavitator, respectively. For both cases, two cavitation numbers (0.3 and 0.4) are simulated and compared with experimental results (Rouse and McNown, 1948). The corresponding Reynolds number are 5.5×10^5 and 6.5×10^5. The comparison shows that the present model and numerical methods predict a reasonable pressure field, especially at the front part of the slender body. The simulation results therefore give the right length of the cavity. The negative pressure coefficient represents the liquid phase changes into vapour phase. After the vapour zone, the pressure is high locally. It suggests that the liquid phase reattaches on the surface of the slender body. Then the pressure recovers to the environmental pressure along the slender body.

4. Numerical simulation for low cavitation number

In general, the cavitation number of supercavitating flow is small, and the size of the cavity is larger than the slender body. In fact, the slender body is immersed in vapour phase. Therefore, it is reasonable to ignore the slender body to simulate the drag and the size of cavity arising from the cavitator. Besides the half-sphere and cone cavitator, a disk cavitator is also frequently adopted in supercavitating flow. The dimensionless supercavity sizes behind a disk cavitator have been plotted in Fig. 5 for both the simulation and experimental results at different cavitation numbers. The length and the maximum diameter of the supercavity (L_c and D_c) are normalized by the diameter of the cavitator (D_n). The numerical results give a similar trend to the experimental results (Knapp et al., 1970). Both the length and the maximum diameter of the supercavity decreases as the cavitation number increases.

Figs. 6 and 7 show the numerical results and experimental measurements of the sizes of the cavity behind a half-sphere and a 45-degree cone cavitator. All of the numerical simulations give a litter larger length and a smaller diameter of the cavity than the corresponding experimental results (Knapp et al., 1970). Furthermore, the diameter of cavity behind the cone and sphere cavitator simulated are more consistent with that of experimental results compared to the disk cavitator. The reason may be that the blockage ratio is larger in numerical simulation than that in experiment. The high blockage ratio suggests that the radical flows are slightly suppressed, it leads to a slight decrease of the radical velocity and an increase of the streamwise velocity. Therefore, the reattachment length increases and the maximum diameter of cavity

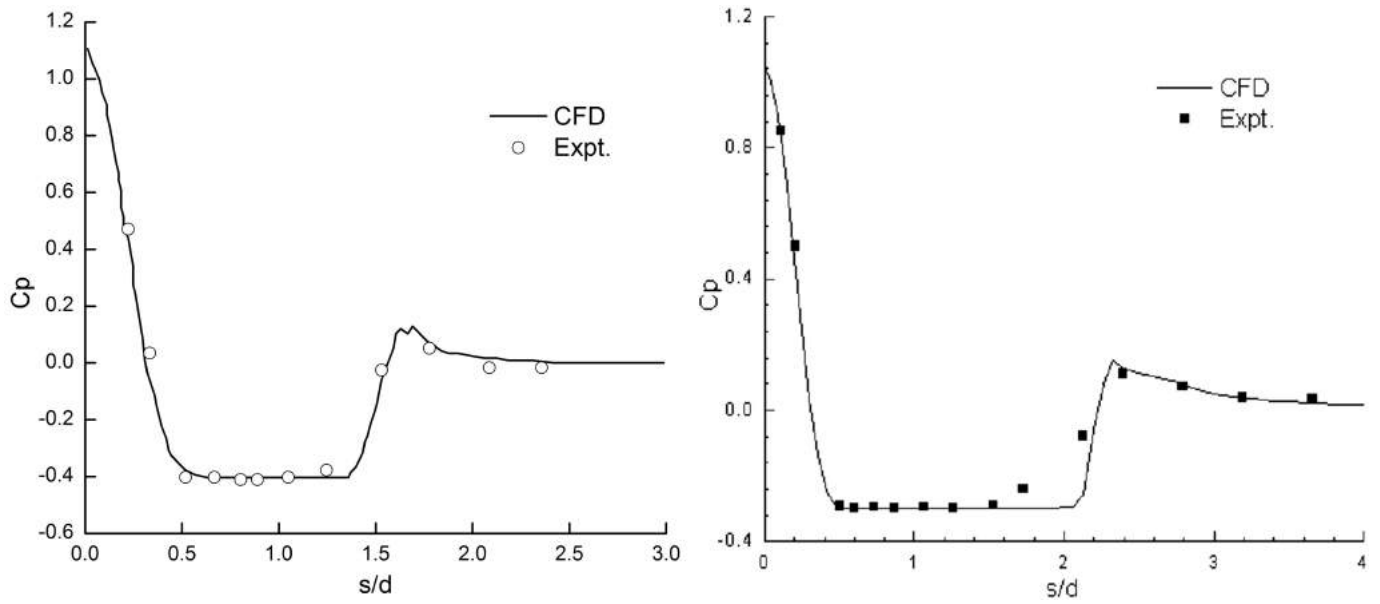

Fig. 3. Comparison of the pressure coefficient around the slender body with a half-sphere cavitator between CFD results and experimental data (left:$\sigma = 0.4$, $\mathrm{Re} = 5.5 \times 10^5$; right:$\sigma = 0.3$, $\mathrm{Re} = 6.5 \times 10^5$).

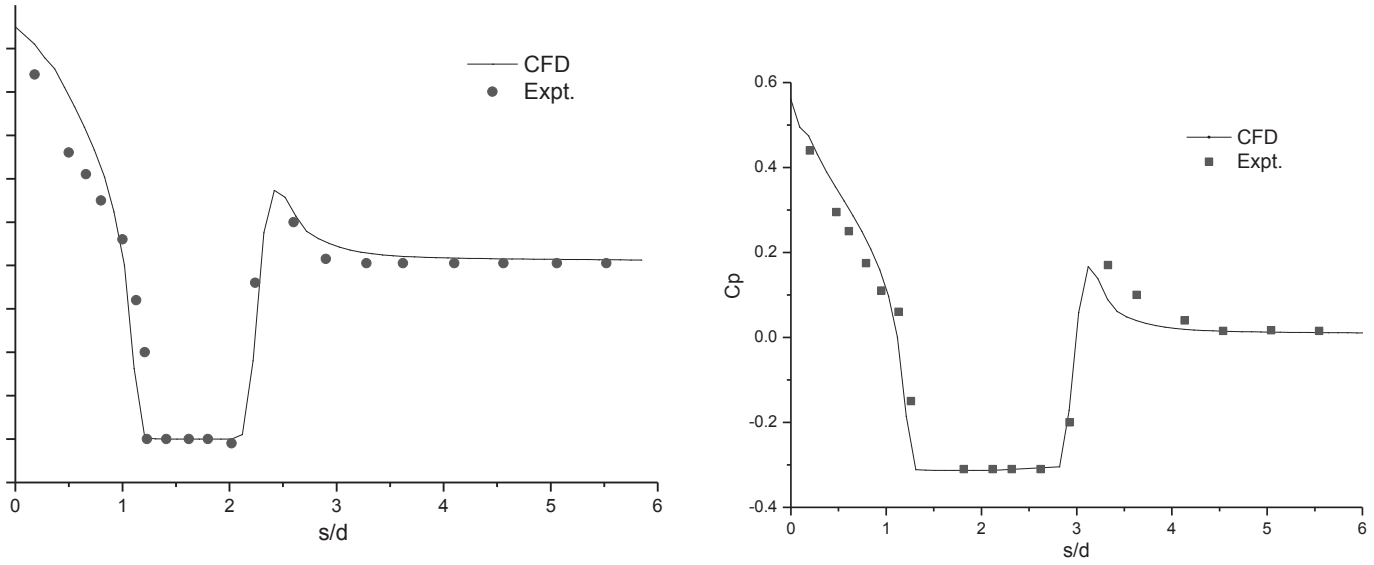

Fig. 4. Comparison of the pressure coefficient around the slender body with a 45-degree cone cavitator between CFD results and experimental data (left:$\sigma = 0.4$, $Re = 5.5 \times 10^5$; right:$\sigma = 0.3$, $Re = 6.5 \times 10^5$).

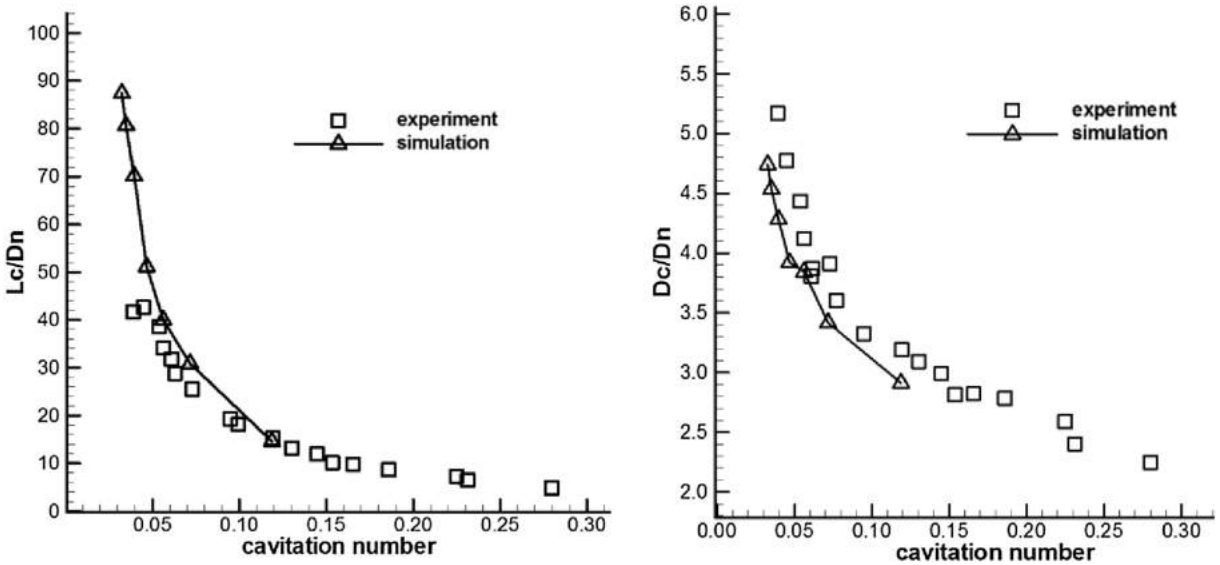

Fig. 5. Supercavity sizes at different cavitation number for disk cavitator (left: the dimensionless length, right: the dimensionless maximum diameter).

decreases. For the disk cavitator, the radical velocity of liquid is larger than that in the other cases, so that it is affected by the blockage ratio more severely than the others.

In Fig. 8, the supercavity outlines behind the three cavitators adopted are plotted at$\sigma = 0.03$. One can observe that the size of cavity arise from the disk cavitator is much larger than the others. The 45-degree cone cavitator produces the smallest cavity. The drag exerted on the cavitator is also important for the supercavitating underwater vehicle, therefore the drag coefficients of the three different cavitators are listed in Tables 1–3. Besides the CFD results, the results of the theoretical prediction by using Reichardt formula ($c_x(\sigma) = c_{x0}(1 + \sigma)$ if$0 < \sigma < 1.2$, c_{x0} is the drag coefficient when cavitation number is 0) are also listed in Tables 1–3 The drag coefficient of disk cavitator is larger than the other two cavitators from the tables. In general, the theoretical prediction of drag coefficient is in a good agreement with the CFD results. It suggests that our numerical results are reliable.

5. Numerical simulation of an unsteady flying SCV

One of the most challenges to investigate the supercavitating flow is the fact that the experimental study is very difficult to implement, since the supercavitation normally occurs at very high speed, which is hard to achieve by using a normal water tunnel. A possible way to perform experimental study is to observe the flow around a fast flying supercavitating object. However, it is very difficult to record more experimental data around an unfixed object except to take images by high speed camera. Hence, an efficient

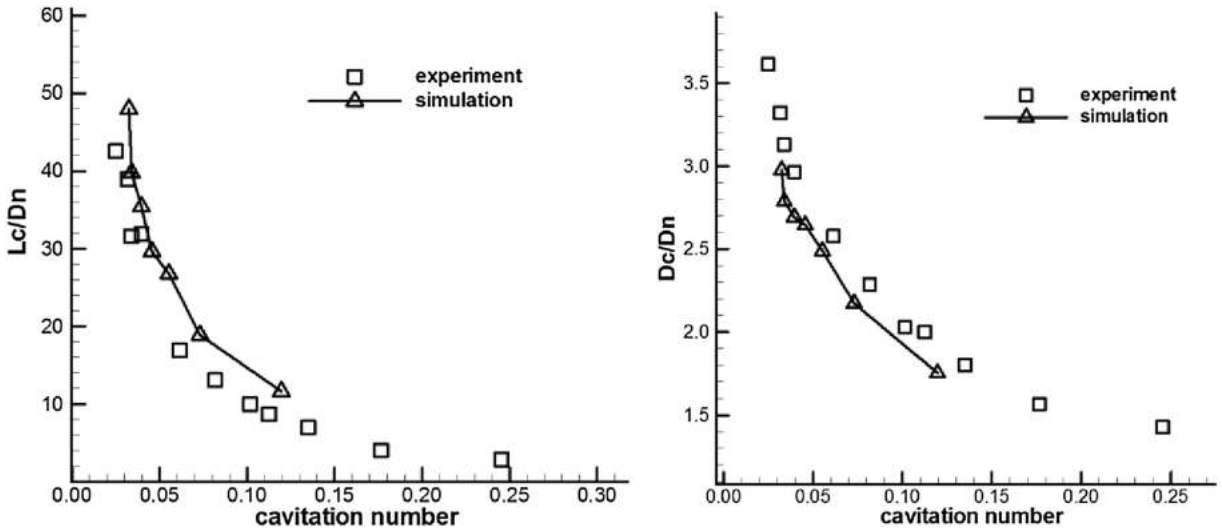

Fig. 6. Supercavity sizes at different cavitation number for half-sphere cavitator (left: the dimensionless length; right: the dimensionless maximum diameter).

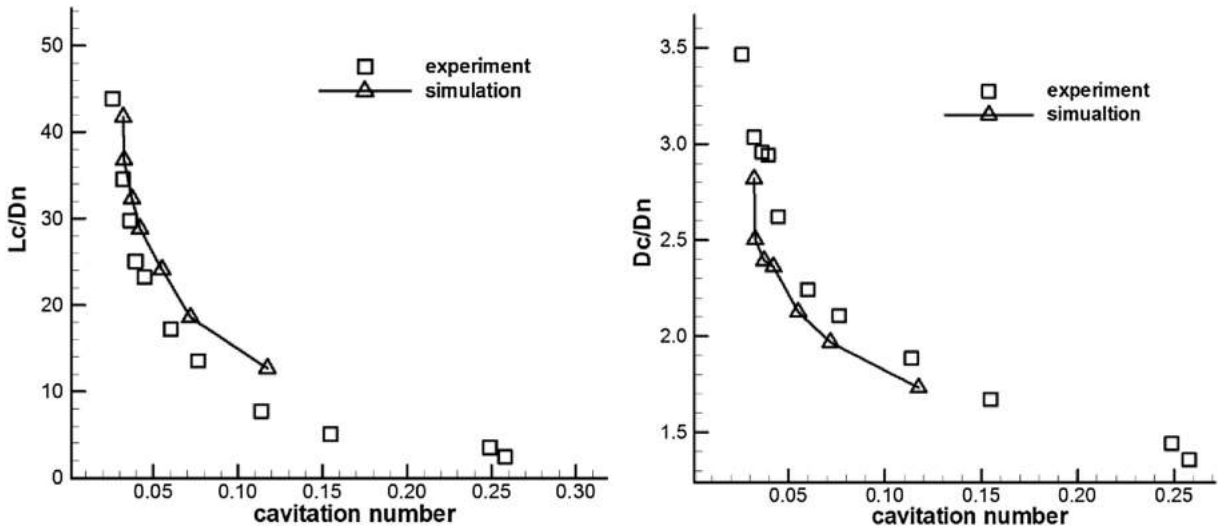

Fig. 7. Supercavity sizes at different cavitation number for cone cavitator (left: the dimensionless length; right: the dimensionless maximum diameter).

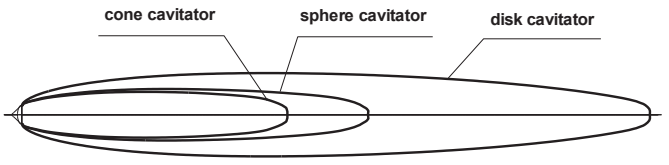

Fig. 8. Supercavity configuration arisen from different cavitators ($\sigma = 0.03$).

Table 1
Drag coefficient of disk cavitator.

Cavitation number	Theory resultsc_x	CFD resultsc_x	Error /%
0.072	0.879	0.886	0.871
0.056	0.866	0.885	2.191
0.047	0.858	0.883	2.921
0.040	0.852	0.880	3.270
0.035	0.849	0.878	3.492
0.033	0.847	0.877	3.621

Table 2
Drag coefficient of half-sphere cavitator.

Cavitation number	Theory resultsc_x	CFD resultsc_x	Error /%
0.120	0.381	0.398	−0.046
0.073	0.365	0.380	−0.042
0.055	0.359	0.368	−0.025
0.046	0.356	0.350	0.014
0.040	0.353	0.346	0.022
0.034	0.352	0.343	0.025
0.032	0.351	0.341	0.029

numerical simulation to compare with the experimental snapshot would be very important. Here we proposal an unsteady simulation by using dynamics mesh to mimic the experimental scenario.

To simulate the unsteady deceleration motion of a SCV, we keep the fluid around SCV at rest in the computation domain, while the vehicle moves at the initial speed of 130 m/s, which

Table 3
Drag coefficient of 45-degree cone cavitator.

Cavitation number	Theory resultsc_x	CFD resultsc_x	Error /%
0.103	0.325	0.337	3.785
0.075	0.309	0.319	3.686
0.059	0.298	0.306	2.627
0.045	0.290	0.296	1.964
0.041	0.288	0.287	−0.177
0.033	0.283	0.281	−0.643
0.030	0.281	0.280	−0.461
0.035	0.284	0.279	−1.913
0.029	0.281	0.274	−2.472

is the same as the launching speed prior to the ignition of a rocket engine in the experiment. However, the length of the water channel is very long compared with the length of the vehicle in the experiment. In the simulation we reduced the length of computational channel and remedied with an auto-moving computational domain. Therefore, the computational cells are generated successively at the beginning of the domain in front of the vehicle and removed at the end of the domain. Consequently, the relative position of the vehicle in the computational domain is approximately fixed. The speed of the moving mesh corresponds to the speed of the vehicle, which is calculated by Newton's second Law$(F_{th} - F_d - \dot{m}V)/m = dV/dt$, where Fth is the thrust act on the vehicle, F_d is the drag of the vehicle, and m is the mass of the vehicle. In the experiment, the vehicle (shown in Fig. 9) is a variable mass system since the solid rocket engine with design thrust of 5 kN is planted inside the vehicle. The initial mass of vehicle is 11.9 kg.

To simplify the dynamical numerical simulation of the SCV, it was assumed that there was no rotational motion during the simulation of the movement of the SCV so that an equilibrium respect to the pitch axis is auto-satisfied. In fact, it is extremely difficult to keep the pitching-moment balance in experiment since the buoyance force of the vehicle exerted by water is lost. This challenge could be overcome in theory by a combination of the following ways: 1) install a flexible nozzle to produce a transverse force in order to balance the gravity of the vehicle; 2) adjust the normal direction of the cavitator slightly; 3) keep the tail of the vehicle contacting with the wall of the cavity to support the gravity of the vehicle; 4) install a set of tail fins extending into liquid zone to stabilize the motion of the vehicle. However, neither the above-mentioned method was adopted in our experiment. Although the pitching-moment is not balanced, a stable horizontal launch with the minimum vibration was strictly controlled. Considering the flying time is short enough in the channel (at the order of 0.1 s), the angular velocity of the vehicle is not very large, thus the SCV flies in the channel. The control of pinching-moment to balance the vehicle will be considered in the future experiment.

To simulate the flying process of the SPV, a moving grid was employed to describe the whole process of the super-cavitation scenario. In the moving grid, the integral form of the conservation equation for a general scalarϕ on an arbitrary control volume V, whose boundary is moving can be written as:

$$\frac{d}{dt}\int_V \rho\phi dV + \int_{\partial V} \rho\phi\left(\vec{u} - \vec{u}_g\right)\cdot d\vec{A} = \int_{\partial V} \Gamma\nabla\phi\cdot d\vec{A} + \int_V \rho S_\phi dV \tag{10}$$

Here ∂V is used to represent the boundary of the control volume V, and u_g is the velocity of the moving mesh. In the simulation, dynamic layering to add or remove layers of cells adjacent to the moving boundary are based on the height of the layer adjacent to the moving surface. The layer of cells adjacent to the moving boundary (layer j in Fig. 10) is split or merged with the layer of cells next to it (layer i in Fig. 10) based on the height (h) of the cells in layer j.

If the cells in layer j are expanding, the cell heights are allowed to increase until:

$$h_{\min} > (1 + \alpha_s)h_{ideal} \tag{11}$$

where h_{min} is the minimum cell height of the cell layer j, h_{ideal} is the ideal cell height, also it is the filter width, and α_s is the layer split factor, 0.3 is used in this study. When this condition is satisfied, the cells are split based on the specified layering options, which are constant height or constant ratio. With the constant height option, the cells are split to create a layer of cells with constant height h_{ideal} and a layer of cells of height (h-h_{ideal}). With the constant ratio option, the cells are split such that the ratio of the new cell heights is exactly the same as everywhere.

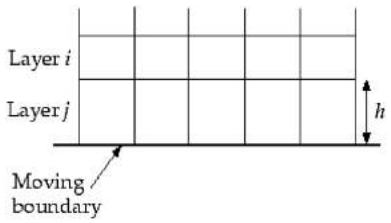

Fig. 10. Dynamic layering.

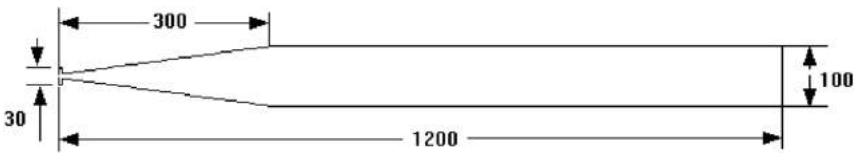

Fig. 9. The geometry of the SCV (unit: mm).

Fig. 11. The mesh around the SCV.

As a result, a hybrid mesh, shown in Fig. 11, is adopted in the simulation. Near the vehicle surface, unstructured grid is used, while the structured grid is used far away the vehicle. It is noted that the exhausted gas with high temperature discharged from the rocket engine may influence the cavitating flow, however, the exhausted gas of the rocket engine is ignored to simplify the computation in the present numerical work, and it need to be studied in the future.

Fig. 12 shows the supercavity of the numerical results and experimental image at the time about 0.02 s. The experimental image is combined by two frames at different time. The vehicle is surrounded by supercavity in both pictures. In both methods, a cavity pinch-off at the rear part was observed. Considering the complexity and safety of experimental measurement, only the speed of the vehicle at fixed locations are measured, the error of the speed between the numerical result and experimental measure is about 1.5% as shown in Fig. 13. The limited comparison suggests that our numerical simulations are qualitatively reasonable.

Here four different unsteady numerical simulations of the SCV are simulated, two of them represent the free fly tests of the vehicle without thrust. On the contrary in the other two simulations, a thrust of 5 Kn is exerted acts on the SCV. In both situations, two cases of the flow, i.e. flows with and without cavitation are simulated. For the flow without cavitation, the cavitation model is switched off. It is noted the flow without cavitation does not suggest an unphysical flow, if the vehicle moves at very high environmental pressure, cavitation would not occur. Fig. 13 shows the speed of vehicle decreases rapidly after launching at the speed of 130 m/s. Especially for the case without cavitation, the speed of vehicle reduces to

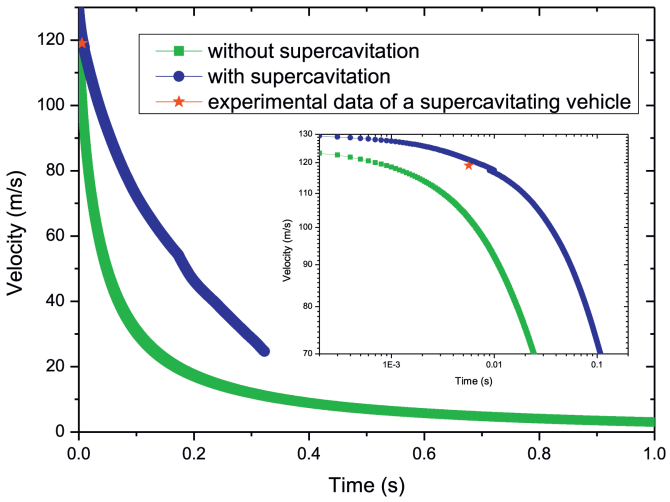

Fig. 13. The speed of the vehicle versus time in the case without thrust (Noted that the horizontal axis is logarithmic).

below 20 m/s in only 0.15 s. The simulation was stopped when the vehicle has moved forward more than 20 m. At the same time, the vehicle with supercavitation still moves at the speed of 25 m/s.

In Fig. 14, the drag coefficients of both cases are plotted. Here the drag coefficient is defined as $c_d = F/0.5\rho V^2 A$, the instantaneous speed of vehicle is served as a reference velocity, A is the streamwise project surface area of the SCV. At the beginning, the drag coefficients are large for both cases, a hydrodynamic explanation for this scenario is the energy consumption of the starting vortex. Subsequently, the drag coefficient keeps at a small value for the case with cavitation. As the speed of the vehicle decreases, the size of the cavity decreases, and the drag coefficient abruptly increases at $t \approx 0.17$ s. On the other hand, the drag coefficient of the vehicle without cavitation keeps increasing. When the vehicle is driven with thrust of 5 kN, the speed of the vehicle decreases at the beginning, then a balance between the drag and thrust is almost achieved as shown in Fig. 15. The ultimate speeds of the vehicle for the case with and without cavitation are 90 m/s and 39 m/s, respectively. It suggests that the supercavitation contributes a drag reduction of 82% for the present case. The drag reduction capacity can also be measured by the drag coefficient shown in Fig. 15.

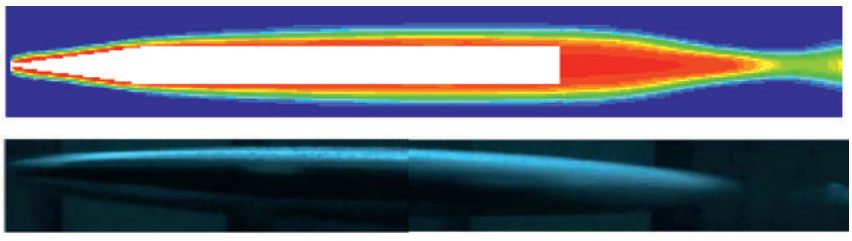

Fig. 12. Numerical result and experimental photo of the supercavity around the vehicle at the time of 0.02 s (+0.007 s) after launching. It should be noted that the whole vehicle is not within the scope of our high-speed camera, so that the experimental photo is combined by two different frames from the video.

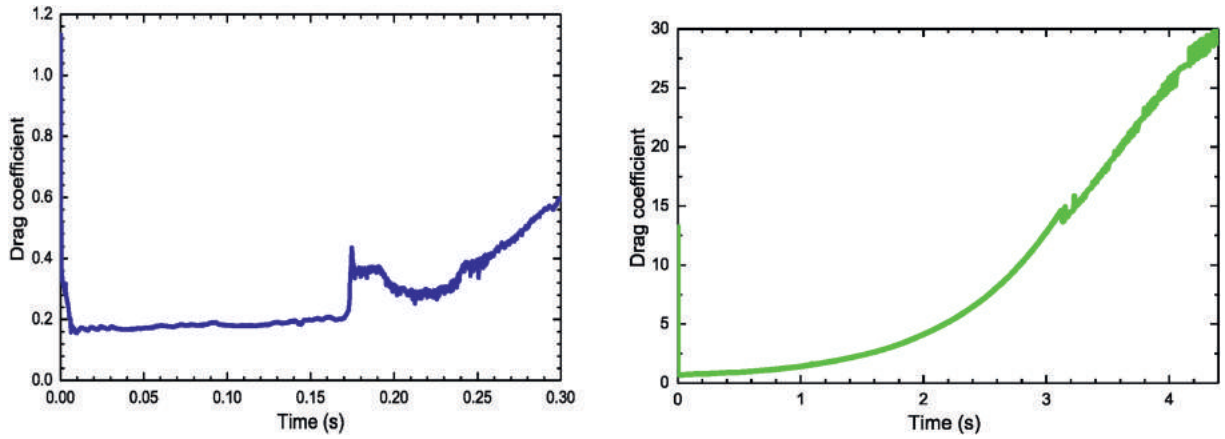

Fig. 14. Drag coefficient of a free flying vehicle with (left) and without (right) cavitation.

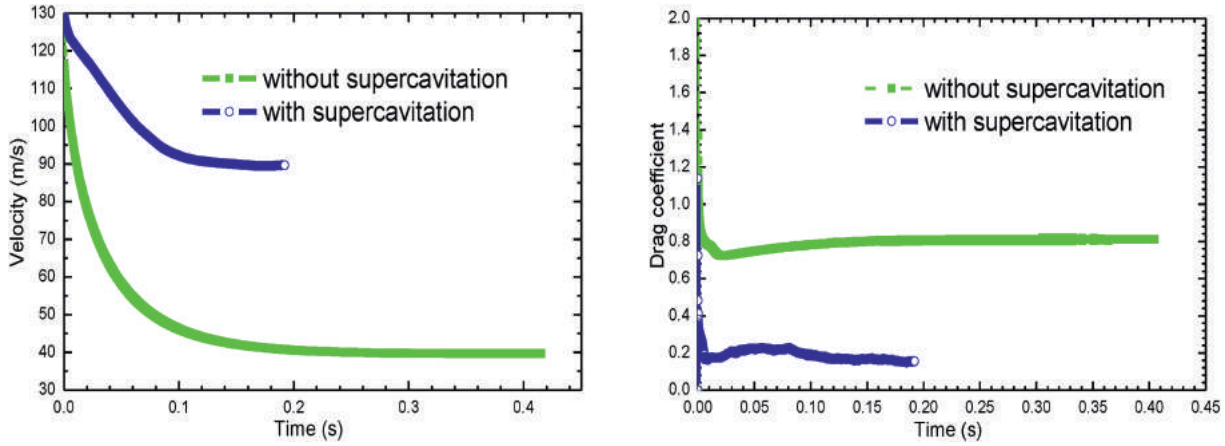

Fig. 15. The speed and the drag coefficient of the vehicle moving with thrust.

6. Concluding remark

Numerical simulation of supercavitating flow is extremely important for the study of SCV. In this manuscript, the SKE turbulent model is modified to avoid the overestimated turbulent viscosity in the mixture of the liquid and vapour phase in supercavitating flow. The numerical results are consistent with experimental results and theoretical predictions, such as the size of supercavity and the drag induced by different cavitators. Furthermore, the computation is more robust with the present numerical method and model.

In the last part of the manuscript, we simulated a fast flying vehicle with and without cavitation in water. The unsteady numerical study shows that the supercavitation can dramatically reduce the resistance force of an underwater vehicle. However, the decrease of the supercavity size can lead to an abruptly drag enhancement. The pinch-off of the cavity are found behind a deceleration vehicle in both the experimental observation and numerical results. The mechanism of the pinch-off of the cavity and the influence of the exhausted jet from the rocket engine on the cavity should be well studied in the future research.

Acknowledgement

This work is supported by National Natural Science Foundation of China (Nos. 11502086 and 11502087) and Fundamental Research Funds for the Central Universities (Nos. 2015QN141, 2015QN018 and 2015MS105).

References

Alyanak, E., Grandhi, R., Penmetsa, R., 2006. Optimum design of a supercavitating torpedo considering overall size, shape, and structural configuration. Int. J. Solids Struct. 43 (3–4), 642–657.

Arndt, R.E.A., 2013. Cavitation research from an international perspective. In: 26th Iahr Symposium Hydraulic Machinery and System, 15. Pts 1–7.

Arndt, R.E.A., Balas, G.J., Wosnik, M., 2005. Control of cavitating flows: a perspective. JSME Int. J. Ser. B-Fluids Therm. Eng. 48 (2), 334–341.

Beaudoin, J.F., Aider, J.L., 2008. Drag and lift reduction of a 3D bluff body using flaps. Exp. Fluids 44 (4), 491–501.

Bruneau, C.H., Chantalat, F., Iollo, A., Jordi, B., Mortazavi, I., 2013. Modelling and shape optimization of an actuator. Struct. Multidiscip. Optim. 48 (6), 1143–1151.

Bruneau, C.H., Mortazavi, I., 2008. Numerical modelling and passive flow control using porous media. Comput. Fluids 37 (5), 488–498.

Cameron, P.J.K., Rogers, P.H., Doane, J.W., Gifford, D.H., 2011. An experiment for the study of free-flying supercavitating projectiles. J. Fluids Eng. Transactions ASME 133 (2).

Ceccio, S.L., 2010. Friction drag reduction of external flows with bubble and gas injection. Annu. Rev. Fluid Mech. 42, 183−203.

Choi, H., Jeon, W.P., Kim, J., 2008. Control of flow over a bluff body. Annual review of fluid mechanics. Palo Alto Annu. Rev. 40, 113−139.

Choi, J.H., Kwak, H.G., Grandhi, R.V., 2005a. Boundary method for shape design sensitivity analysis in solving free-surface flow problems. J. Mech. Sci. Technol. 19 (12), 2231−2244.

Choi, J.H., Penmetsa, R.C., Grandhi, R.V., 2005b. Shape optimization of the cavitator for a supercavitating torpedo. Struct. Multidiscip. Optim. 29 (2), 159−167.

Coutier-Delgosha, O., Deniset, F., Astolfi, J.A., Leroux, J.B., 2007. Numerical prediction of cavitating flow on a two-dimensional symmetrical hydrofoil and comparison to experiments. J. Fluids Eng. Transactions ASME 129 (3), 279−292.

Dieval, L., Pellone, C., Franc, J.P., Arnaud, M., 2000. A tracking method for the modeling of attached cavitation. Comptes Rendus De. L Acad. Des. Sci. Ser. Ii Fasc. B-Mecanique 328 (11), 809−812.

Gao, G.H., Zhao, J., Ma, F., Luo, W.D., 2012. Numerical study on ventilated supercavitation reaction to gas supply rate. Mater. Process. Technol. 418−420, 1781−1785. Pts 1−3.

Hrubes, J.D., 2001. High-speed imaging of supercavitating underwater projectiles. Exp. Fluids 30 (1), 57−64.

Ito, J., Tamura, J., Mikata, M., 2002. Lifting-line theory of a supercavitating hydrofoil in two-dimensional shear flow − (Application to partial cavitation). JSME Int. J. Ser. Therm. Eng. 45 (2), 287−292.

Kim, S., Kim, N., 2015. Integrated dynamics modeling for supercavitating vehicle systems. Int. J. Nav. Archit. Ocean Eng. 7 (2), 346−363.

Knapp, R.T., Daily, J.W., Hammit, F.G., 1970. Cavitation. McGraw-Hill. Inc.

Kulagin, V.A., 2002. Analysis and calculation of a flow in a supercavitation mixer. Chem. Petroleum Eng. 38 (3−4), 207−211.

Likhachev, D.S., Li, F.C., 2014. Numerical study of the characteristics of supercavitation on a cone in a stationary evaporator. Desalination Water Treat. 52 (37−39), 7053−7064.

Nouri, N.M., Eslamdoost, A., 2009. An iterative scheme for two-dimensional supercavitating flow. Ocean. Eng. 36 (9−10), 708−715.

Pan, S.L., Zhou, Q., 2014. Natural supercavitation characteristic simulation of small-caliber projectile. Mater. Sci. Civ. Eng. Archit. Sci. Mech. Eng. Manuf. Technol. 488−489, 1243−1247. Pts 1 and 2.

Rouse, H., McNown, J.S., 1948. Cavitation and Pressure Distribution, Head Forms at Zero Angle of Yaw. Iowa Institute of Hydraulic Research, State Univ. of Iowa, Iowa City.

Seif, M.S., Asnaghi, A., Jahanbakhsh, E., 2009. Drag force on a flat plate in cavitating flows. Pol. Marit. Res. 16 (3), 18−25.

Singhal, A.K., Athavale, M.M., Li, H.Y., Jiang, Y., 2002. Mathematical basis and validation of the full cavitation model. J. Fluids Eng. Transactions ASME 124 (3), 617−624.

Tulin, M.P., 1998. On the shape and dimensions of three-dimensional cavities in supercavitating flows. Appl. Sci. Res. 58 (1−4), 51−61.

Xiong, Y.L., Bruneau, C.H., Kellay, H., 2010. Drag enhancement and drag reduction in viscoelastic fluid flow around a cylinder. EPL 91 (6).

Xiong, Y.L., Bruneau, C.H., Kellay, H., 2013. A numerical study of two dimensional flows past a bluff body for dilute polymer solutions. J. Newt. Fluid Mech. 196, 8−26.

Yi, W.J., Tan, J.J., Xiong, T.H., 2009. Investigations on the drag reduction of high-speed natural supercavitation bodies. Mod. Phys. Lett. B 23 (3), 405−408.